Electronic Supplementary Material (ESI) for Green Chemistry.
This journal is © The Royal Society of Chemistry 2023

Compositionally modulated FeMn bimetallic skeletons for highly efficient overall water splitting†

Licheng Huang,‡[a] Ruiqi Yao,‡[b] Zili Li,[d] Jiaxin He,[a] Yingqi Li,*[b] Hongxiang Zong,*[c] Shuang Han,*[a] Jianshe Lian,[a] Yangguang Li[b] and Xiangdong Ding[c]

[a.]Key Laboratory of Automobile Materials, Ministry of Education, School of Materials Science and Engineering, Jilin University, Changchun 130022, China. E–mail: shuanghan@jlu.edu.cn

[b.]Key Laboratory of Polyoxometalate and Reticular Material Chemistry of Ministry of Education, Faculty of Chemistry, Northeast Normal University, Changchun 130024, China. E–mail: liyq164@nenu.edu.cn

[c.]State Key Laboratory for Mechanical Behavior of Materials, Xi'an Jiaotong University, Xi'an 710049, China. E–mail: zonghust@xjtu.edu.cn

[d.]Vaccine Room 1, Changchun Institute of Biological Products Co Ltd, Changchun 130022, PR China.

‡.The first two authors contributed equally to this work.

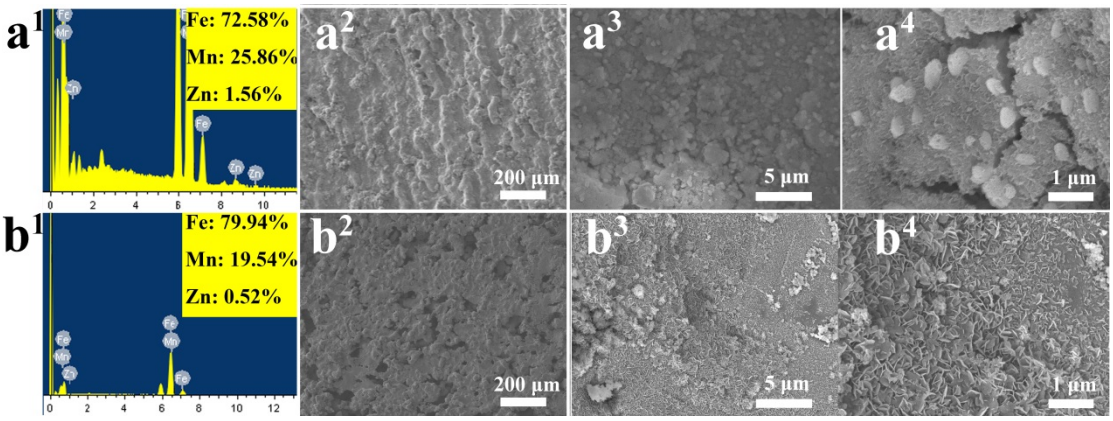

Figure S1. EDS spectra of (a^1) FMZ1 and (b^1) FMZ2; SEM images of (a^2–a^4) FMZ1 and (b^2–b^4) FMZ2.

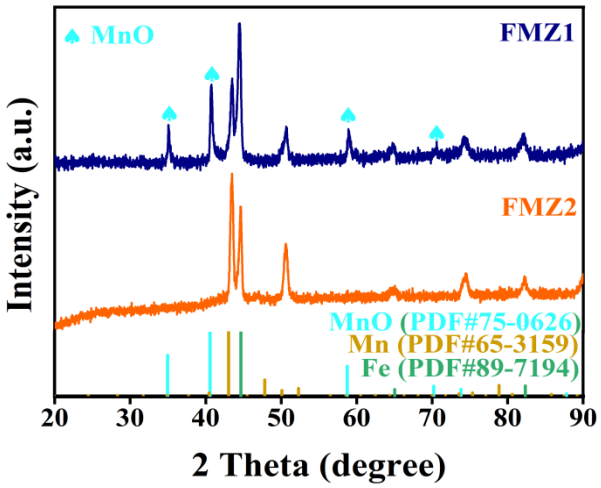

Figure S2. XRD patterns of FMZ1 and FMZ2.

In **Figure S2**, the diffraction peaks of FMZ1 correspond to metallic Fe, Mn and MnO (PDF#75–0626), where the diffraction peak of MnO is specially marked. After etching, the diffraction peaks of MnO disappear while the peaks of both metallic Fe and Mn are retained. The absence of any significant metallic Zn peaks both before and after etching is due to the low content, but the Zn content can be traced by energy dispersive spectrometer (EDS) spectrum. The proportion of Mn and Zn in FMZ2 decreases while the proportion of Fe element increases compared to FMZ1 (**Figure S1a^1 and b^1**), which also indicates that the elements in FMZ1 are selectively etched.

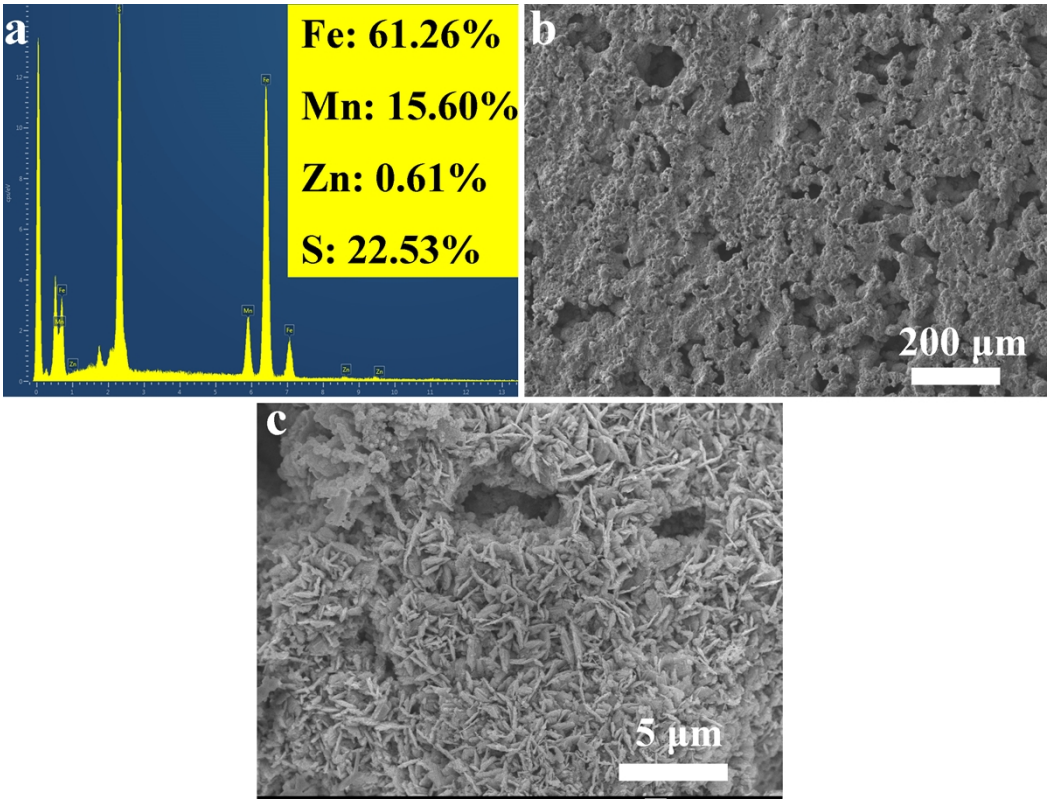

Figure S3. (a) EDS spectra of FMZS2; (b, c) SEM images of FMZS2.

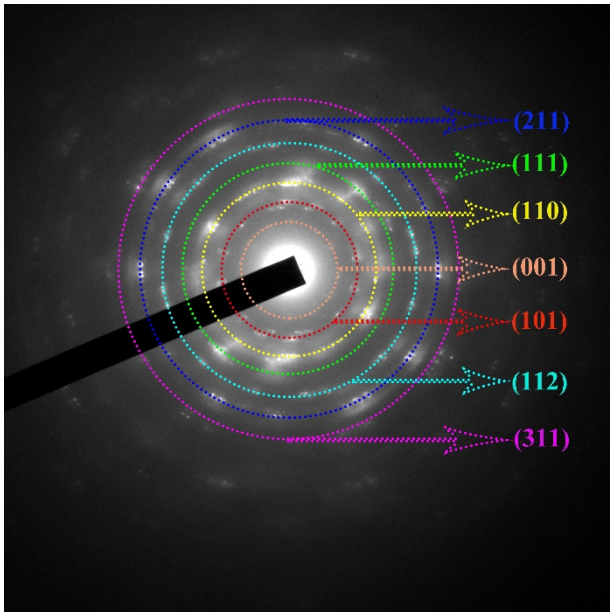

Figure S4. SAED pattern of FMZS2.

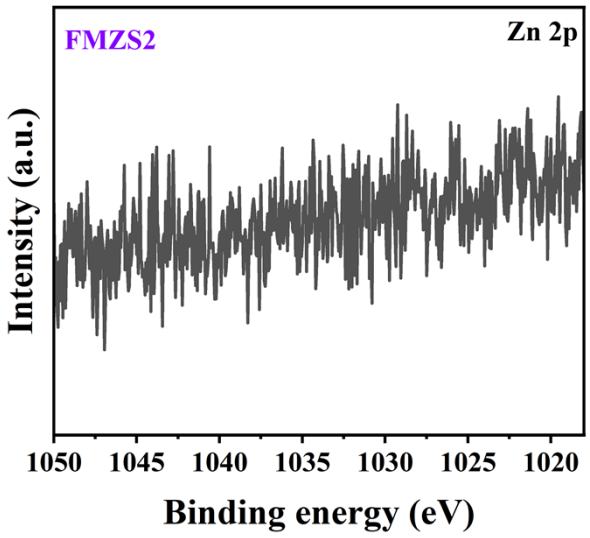

Figure S5. High–resolution spectra of Zn 2*p* for FMZS2.

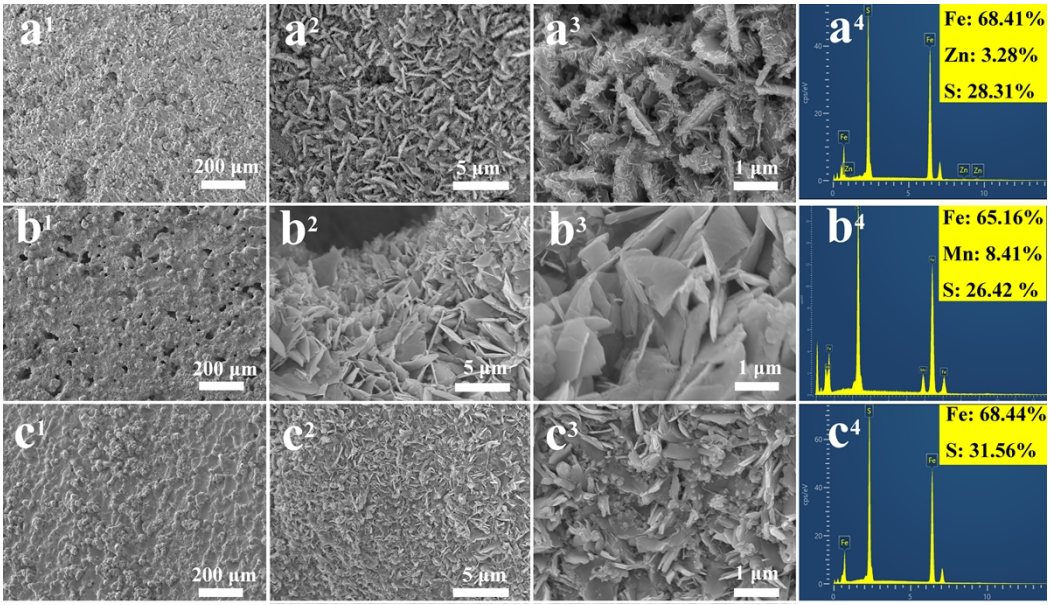

Figure S6. SEM images of (a^1–a^3) FZS2, (b^1–b^3) FMS2 and (c^1–c^3) FS2; EDS spectra of (a^4) FZS2, (b^4) FMS2 and (c^4) FS2.

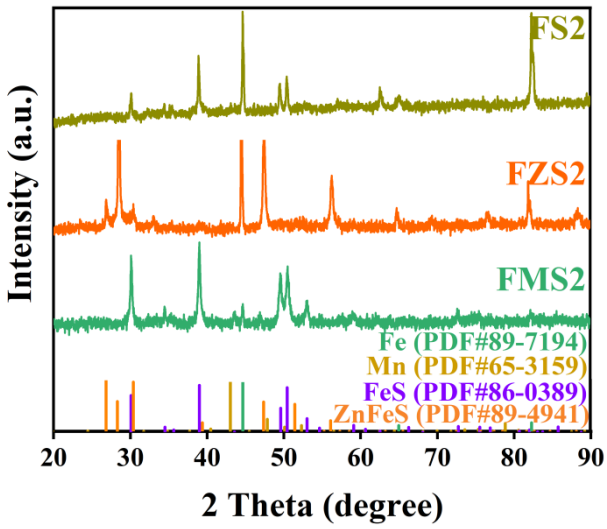

Figure S7. XRD patterns of FS2, FZS2 and FMS2.

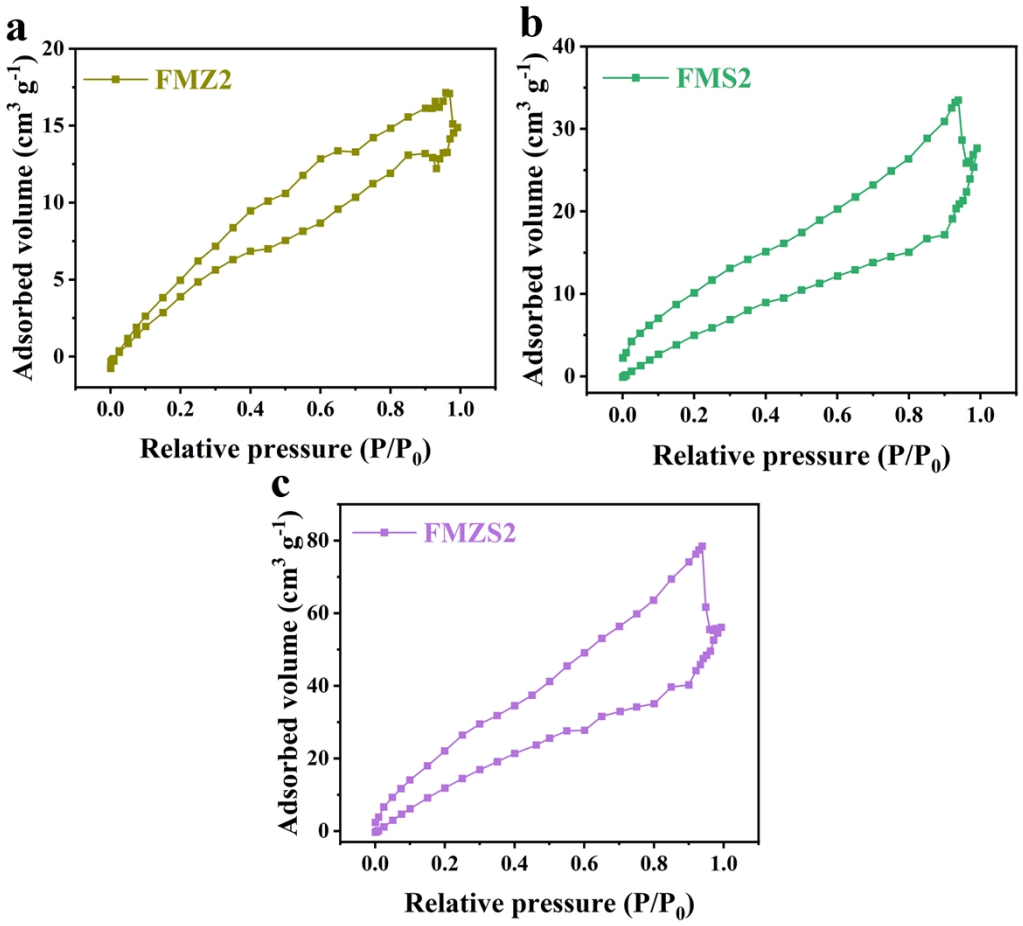

Figure S8. Nitrogen adsorption-desorption isotherms of (a) FMZ2, (b) FMS2 and (c) FMZS2.

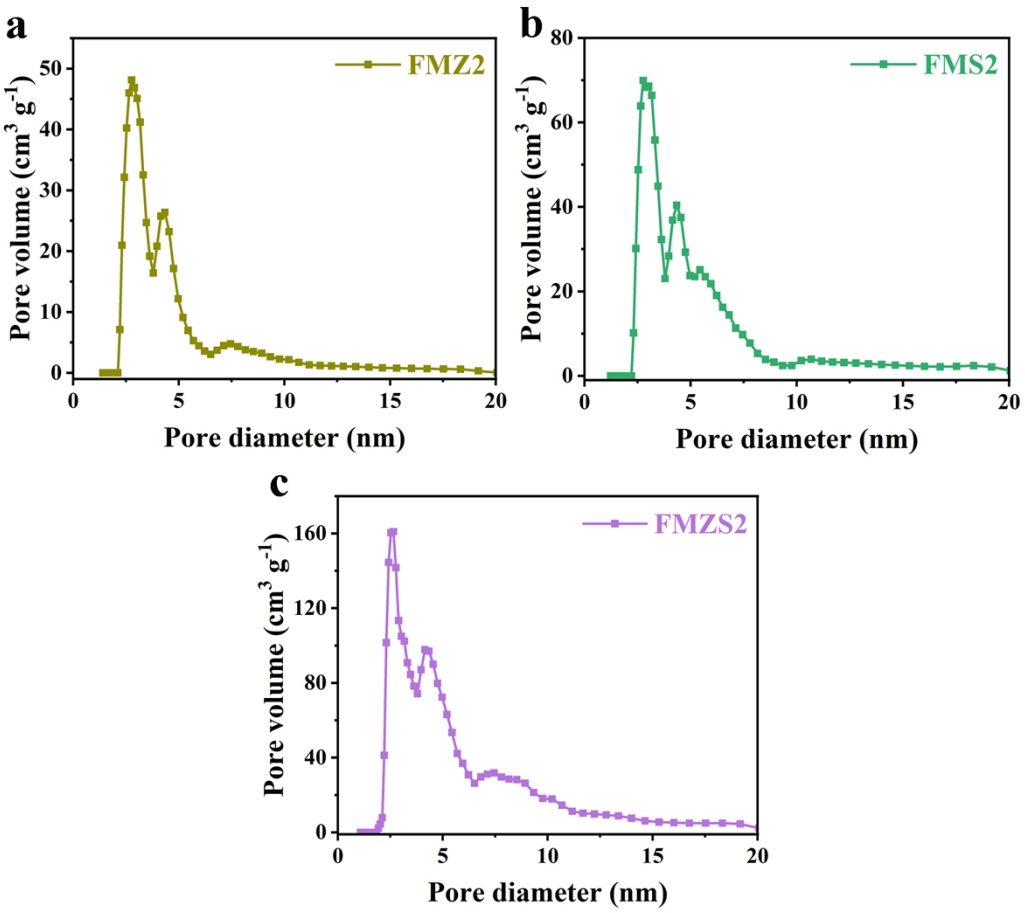

Figure S9. Pore diameters of (a) FMZ2, (b) FMS2 and (c) FMZS2.

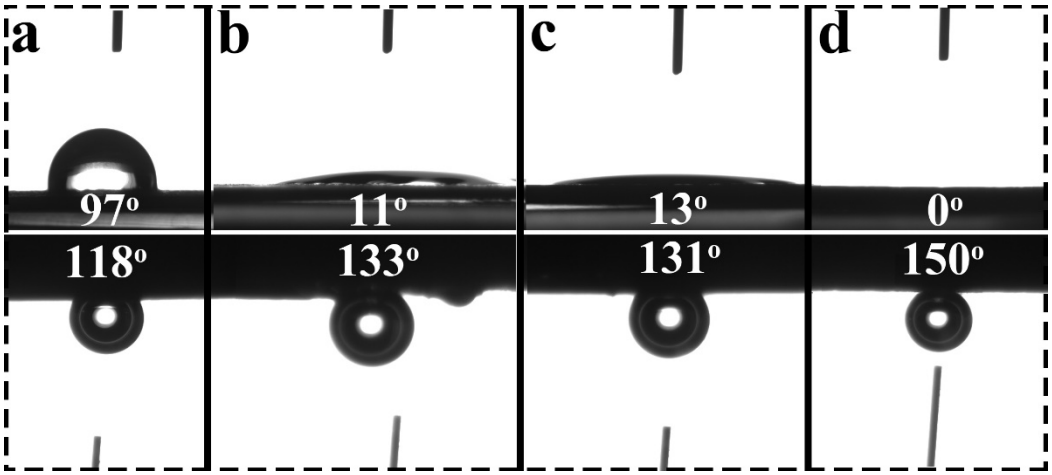

Figure S10. In–air water (top) and underwater bubble (below) contact angle of (a) FS2, (b) FZS2, (c) FMS2 and (d) FMZS2.

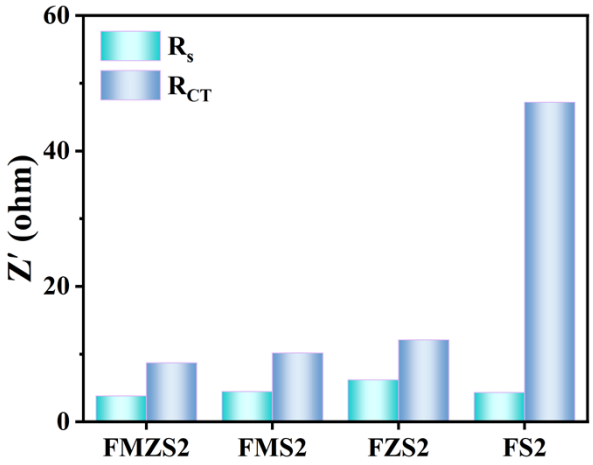

Figure S11. Comparison of intrinsic resistance and charge transfer resistance of FMZS2, FMS2, FZS2 and FS2 according to EIS analysis in 1 M KOH solution.

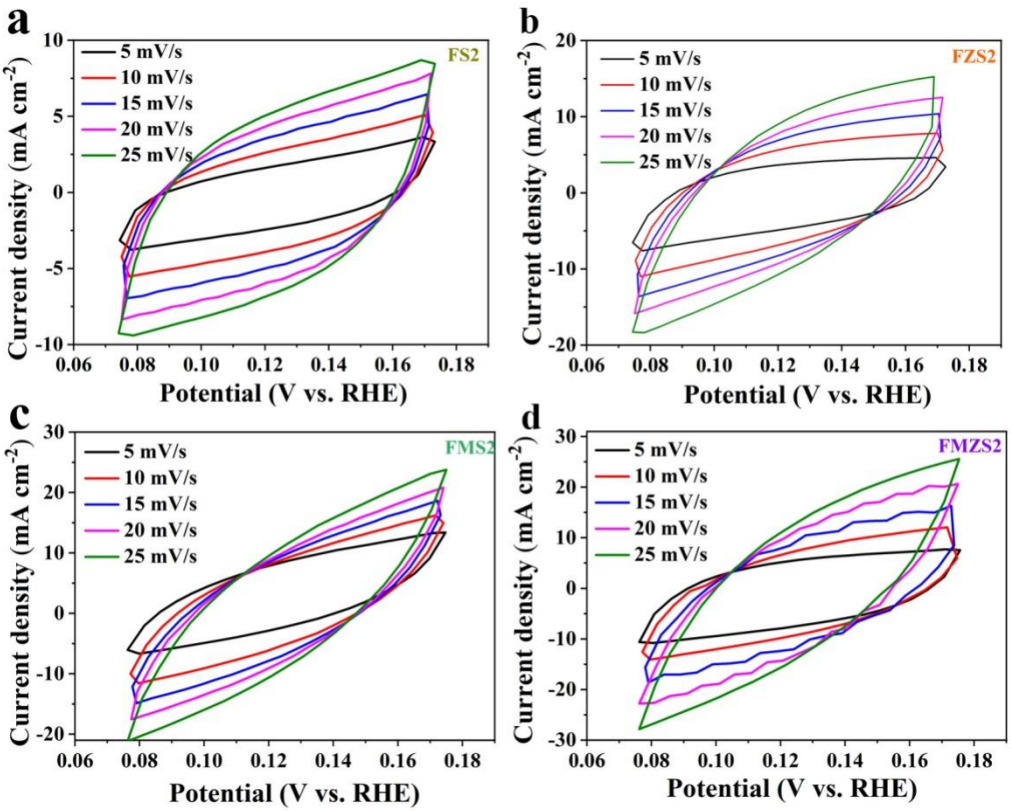

Figure S12. CV curves in the potential ranging from 0.074 to 0.174 V for (a) FS2, (b) FZS2, (c) FMS2 and (d) FMZS2 at various scan rates.

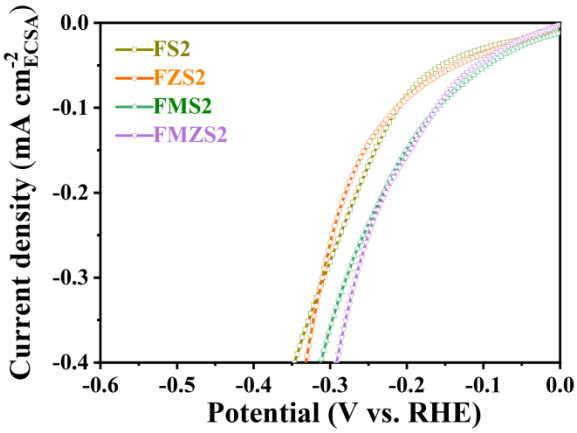

Figure S13. HER activity of FS2, FZS2, FMS2 and FMZS2 in 1 M KOH normalized by ECSA.

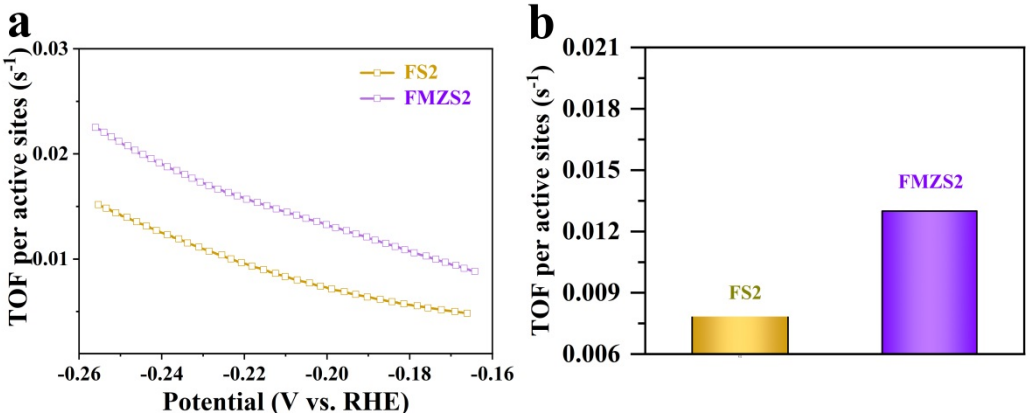

Figure S14. (a) TOF values as a function of potential for FS2 and FMZS2; (b) TOF values of FS2 and FMZS2 at the overpotential of 200 mV.

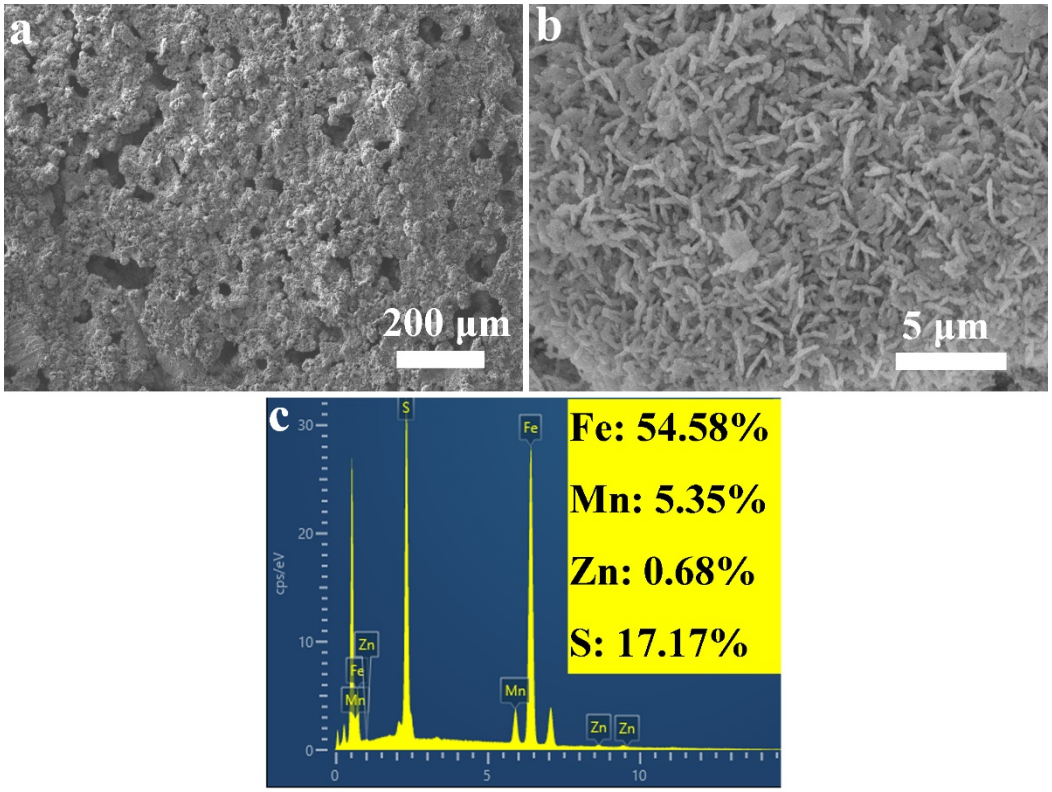

Figure S15. SEM images of (a, b) FMZS2 after 30 h HER; EDS spectra of (c) FMZS2 after 30 h HER.

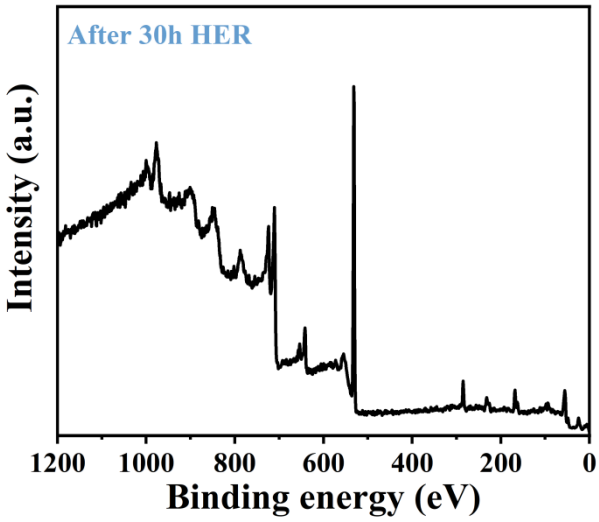

Figure S16. XPS survey spectra of FMZS2 after 30 h HER.

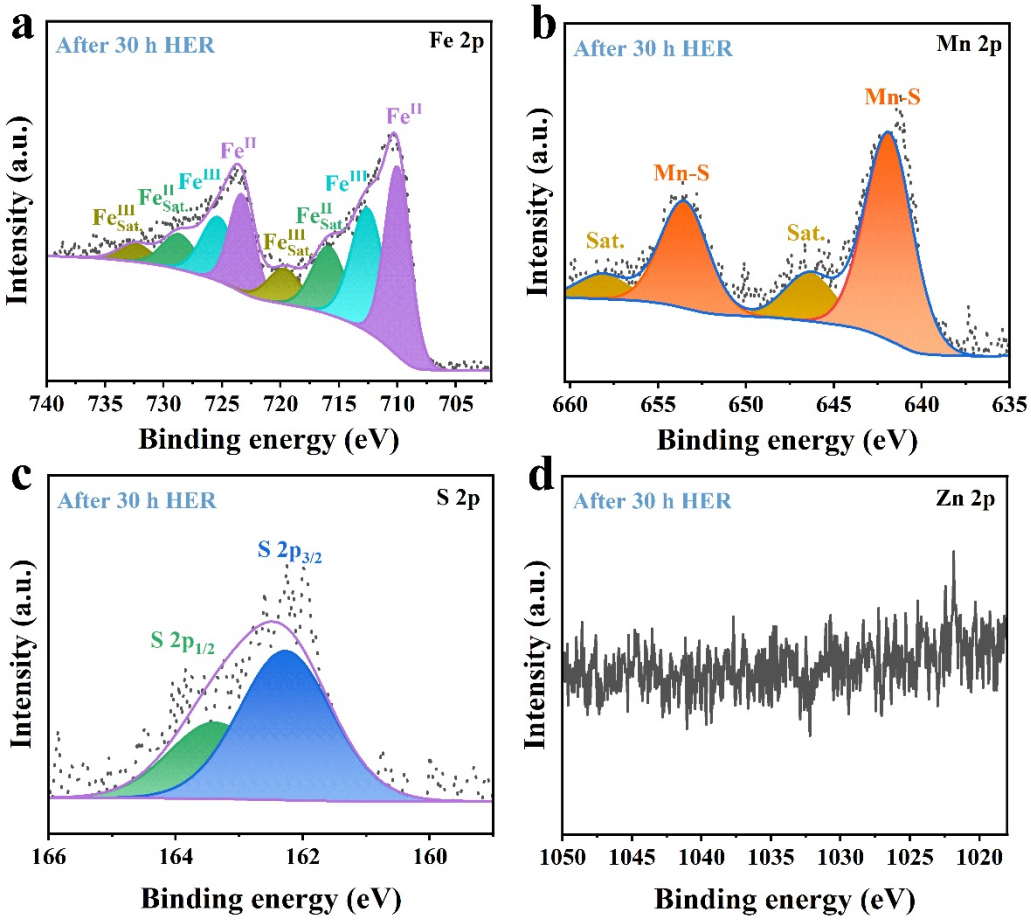

Figure S17. XPS spectra of (a) Fe 2p, (b) Mn 2p, (c) S 2p and (d) Zn 2p for FMZS2 after 30 h HER.

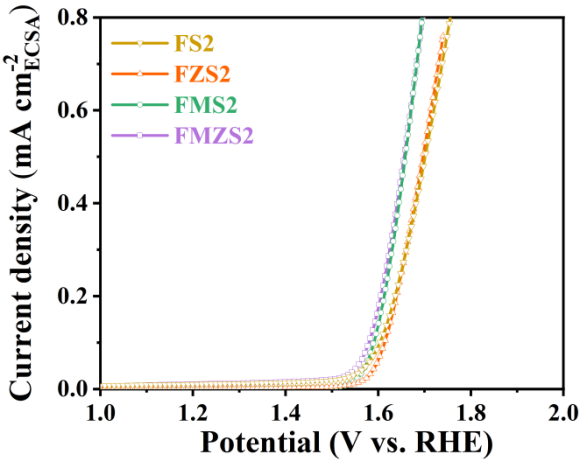

Figure S18. OER activity of FS2, FZS2, FMS2 and FMZS2 in 1 M KOH normalized by ECSA.

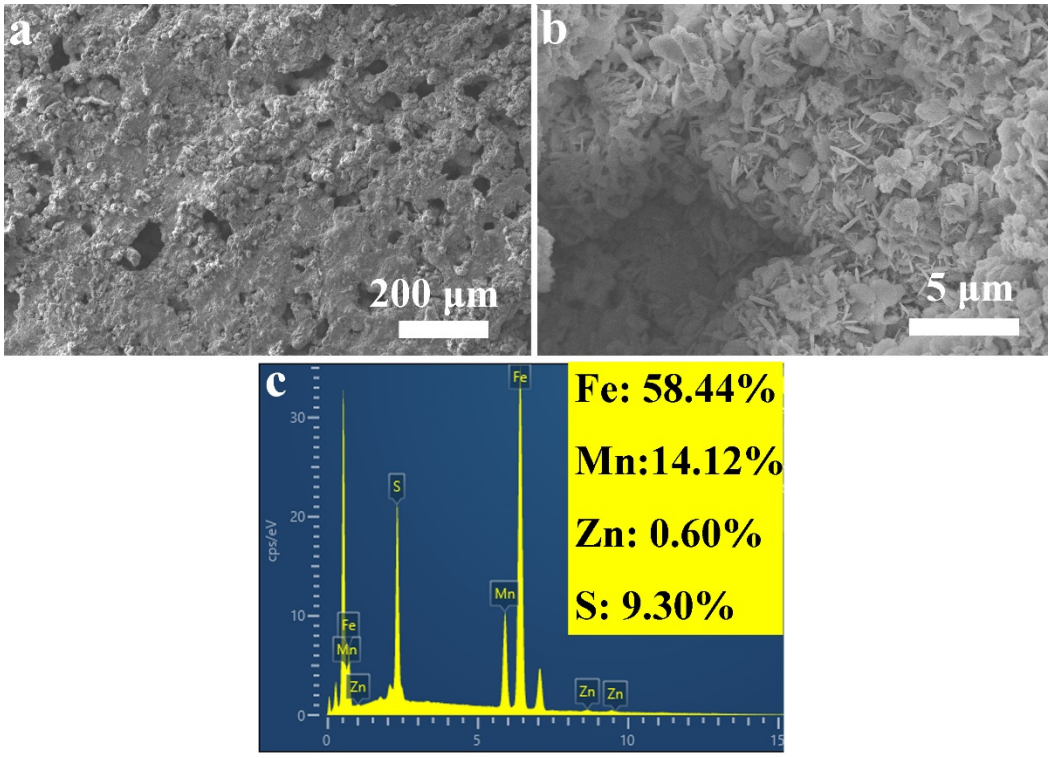

Figure S19. SEM images of (a, b) FMZS2 after 30 h OER; EDS spectra of (c) FMZS2 after 30 h OER.

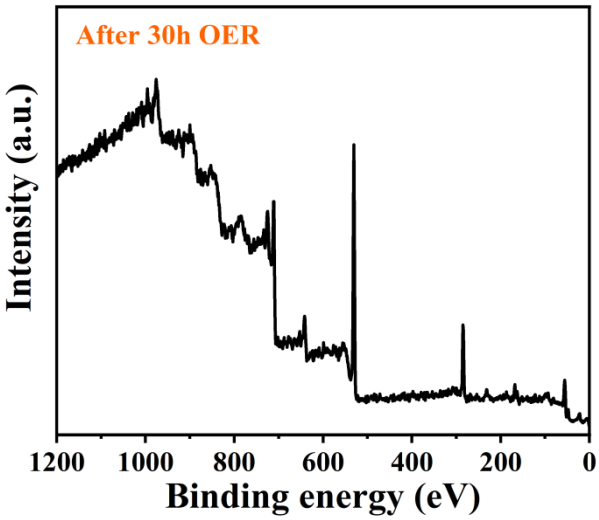

Figure S20. XPS survey spectra of FMZS2 after 30 h OER.

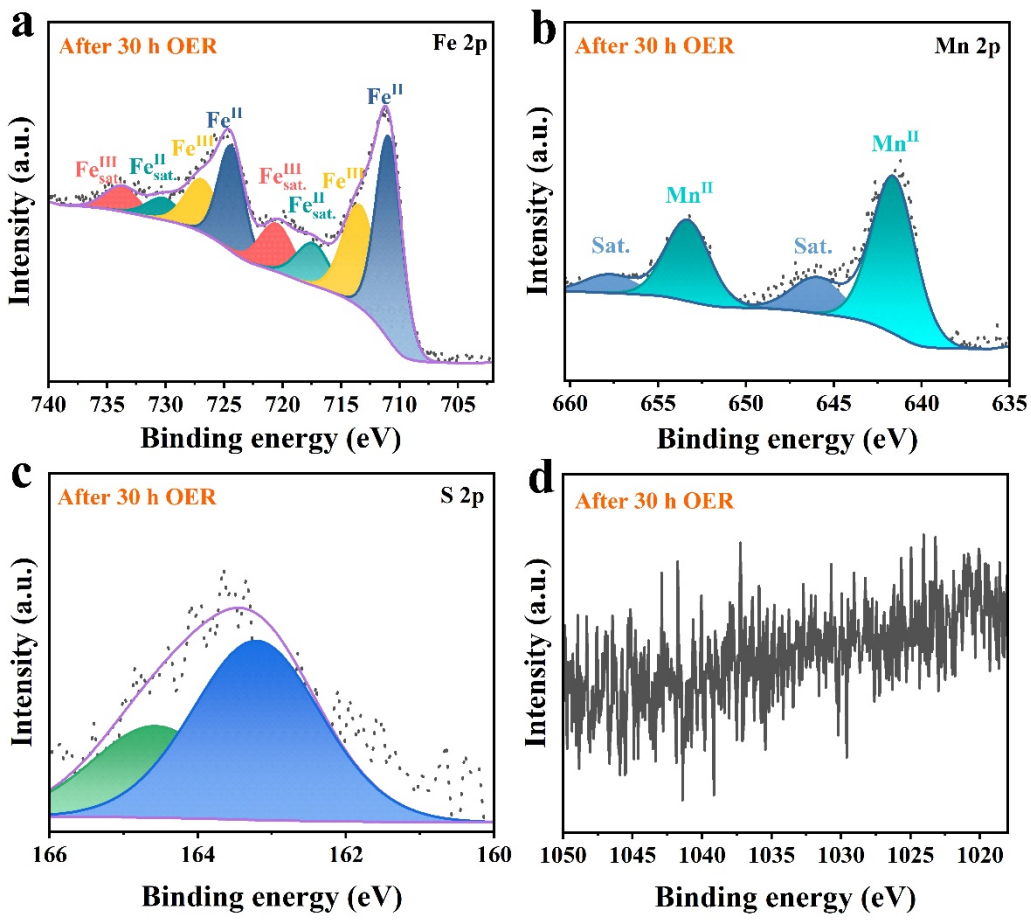

Figure S21. XPS spectra of (a) Fe 2p, (b) Mn 2p, (c) S 2p and (d) Zn 2p for FMZS2 after 30 h OER.

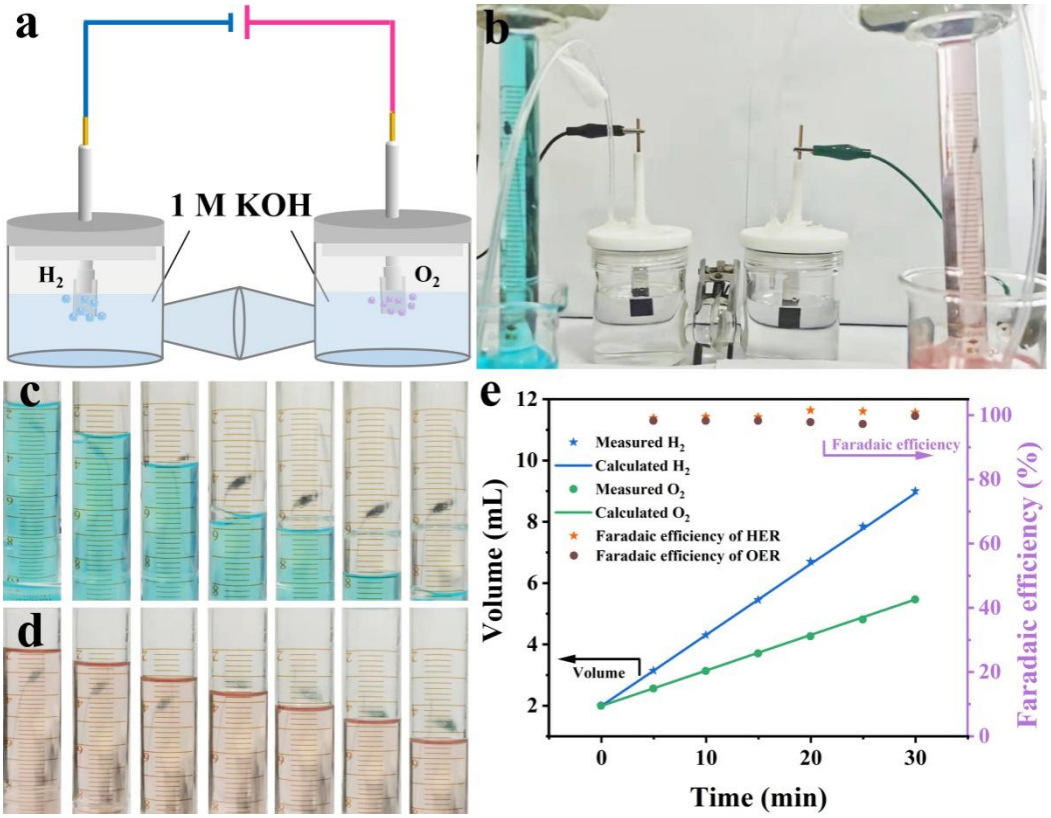

Figure S22. (a) Schematic of the electrolyzed water reaction. The cathodic and anodic reaction vessels are separated by Nafion membrane (b) Digital photograph of the gas collection device, wherein two measuring cylinders are connected to the reaction vessels via gas circuit. (c) Hydrogen and (d) oxygen generated at 0, 5, 10, 15, 25 and 30 min, respectively; (e) Experimental and theoretical gas volumes of H_2 and O_2 during water splitting at a current density of 30 mA cm^{-2} for 30 min, and the corresponding Faradaic efficiency of FMZS2.

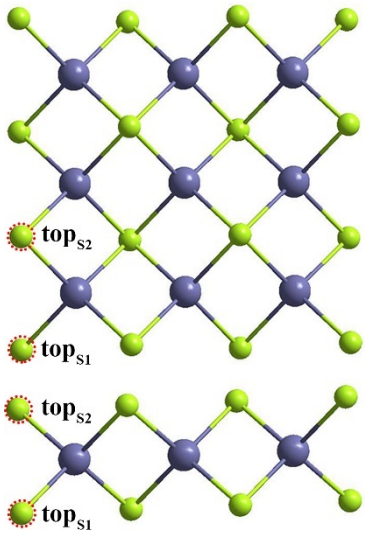

Figure S23. Top view (top) and side view (below) slab model of FS2.

Table S1 ICP-OES results of FMZS2.

electrocatalyst	Fe (ug/mL)	Mn (ug/mL)	Zn (ug/mL)
FMZS2	1.554051	0.549994	0.038375

Table S2 BET and pore diameters result of FMZ2, FMS2 and FMZS2.

Electrocatalyst	BET (m^2 g^{-1})	Pore diameter-1 (nm)	Pore diameter-2 (nm)
FMZ2	62.40	3.030	4.2772
FMS2	87.5	3.169	4.3502
FMZS2	147.8	2.647	4.2498

Table S3 Comparison of the HER performance of reported electrocatalysts.

Electrocatalyst	Electrolyte	Overpotential	Current density	Ref.
FeMnZn/Mn-FeS	**1 M KOH**	**118 mV**	20 mA cm^{-2}	**This work**
$Fe_{1-x}Co_xS_2$/CNT	1 M KOH	120 mV	20 mA cm^{-2}	1
NiO_x NPs	1 M KOH	174 mV	20 mA cm^{-2}	2
Co_2P	1 M KOH	171 mV	20 mA cm^{-2}	3
CNTs@NiP_2/NiP	1 M KOH	137 mV	20 mA cm^{-2}	4
FeCoNi–LTH/$NiCo_2O_4$/CC	1 M KOH	151 mV	20 mA cm^{-2}	5
Cu@Cu_2S	1 M KOH	203 mV	20 mA cm^{-2}	6
VC–NS	1 M KOH	120 mV	20 mA cm^{-2}	7
MoP/Mo_2N	1 M KOH	165 mV	20 mA cm^{-2}	8
Co_2P	1 M KOH	167 mV	20 mA cm^{-2}	3
$Ni(OH)_2$	1 M KOH	170 mV	20 mA cm^{-2}	9
m–NiS_x–0.5/NF	1 M KOH	137 mV	20 mA cm^{-2}	10
Ni–NiO/N–rGO	1 M KOH	160 mV	20 mA cm^{-2}	11
CoS_x–Ni_3S_2/NF	1 M KOH	146 mV	20 mA cm^{-2}	12
Ni_3S_2/Co_3S_4	1 M KOH	150 mV	20 mA cm^{-2}	13
$NiCo_2O_4$	1 M KOH	160 mV	20 mA cm^{-2}	14
Co–B/Ni	1 M KOH	200 mV	20 mA cm^{-2}	15
Co_3O_4/MoS_2	1 M KOH	221 mV	20 mA cm^{-2}	16
MoS_2/NiCo–LDH	1 M KOH	130 mV	20 mA cm^{-2}	17
EG/$Co_{0.85}Se$/NiFe–LDH	1 M KOH	350 mV	20 mA cm^{-2}	18

Table S4 Comparison of the OER performance of reported electrocatalysts.

Electrocatalyst	Electrolyte	Overpotential	Current density	Ref.
FeMnZn/Mn-FeS	**1 M KOH**	**390 mV**	**100 mA cm^{-2}**	**This work**
$Cu(OH)_2$/Cu	1 M KOH	390 mV	100 mA cm^{-2}	19
MCo_2O_4@MCo_2S_4@PPy	1 M KOH	395 mV	100 mA cm^{-2}	20
CuO NCA	1 M KOH	400 mV	100 mA cm^{-2}	21
Pd	1 M KOH	400 mV	100 mA cm^{-2}	22
N–FeP	1 M KOH	440 mV	100 mA cm^{-2}	23
Fe_7S_8/NGF	1 M KOH	450 mV	100 mA cm^{-2}	24
Ni_2Mo_3N/NF	1 M KOH	392 mV	100 mA cm^{-2}	25
$MoSe_2$–Ni_3Se_2/NF	1 M KOH	395 mV	100 mA cm^{-2}	[26]
CoFe–LDH /$CoFe_2O_4$/NF	1 M KOH	400 mV	100 mA cm^{-2}	27
BSeF/$Ni(OH)_2$	1 M KOH	401 mV	100 mA cm^{-2}	28
NiCo–LDH	1 M KOH	410 mV	100 mA cm^{-2}	29
FeNi/NF	1 M KOH	422 mV	100 mA cm^{-2}	30
$Co_3V_2O_8$	1 M KOH	497 mV	100 mA cm^{-2}	31
Mo/P@Co_3O_4	1 M KOH	418 mV	100 mA cm^{-2}	32
$NiCo_2O_4$– $NiCo(OH)_x$	1 M KOH	484 mV	100 mA cm^{-2}	33
CuCo–Ni_3S_2/NF	1 M KOH	400 mV	100 mA cm^{-2}	34
Ni–Mo–Fe	1 M KOH	408 mV	100 mA cm^{-2}	35
$FeCoNiB_x$	1 M KOH	419 mV	100 mA cm^{-2}	36
TiO_2/Ti_3C_2/FeNi LDH	1 M KOH	633 mV	100 mA cm^{-2}	37

Table S5 Comparison of the overall water splitting performance of reported catalysts.

Catalyst	Electrolyte	Overpotential	Current density	Ref.
FeMnZn/Mn-FeS	**1 M KOH**	**1.62 V**	**10 mA cm^{-2}**	**This work**
NF	1 M KOH	1.65 V	10 mA cm^{-2}	38
Ni_3Se_2	1 M KOH	1.65 V	10 mA cm^{-2}	39
xNiP@SS	1 M KOH	1.77 V	10 mA cm^{-2}	40
CoP@NF||CoP/CoO@NF	1 M KOH	1.62 V	10 mA cm^{-2}	41
CoP/VGNHs	1 M KOH	1.63 V	10 mA cm^{-2}	42
CoS_2/CC	1 M KOH	1.66 V	10 mA cm^{-2}	43
Co_2N/TM/Co–Pi/TM	1 M KOH	1.78 V	10 mA cm^{-2}	44
$Co_{0.4}Fe_{0.6}$ LDH/g–CNx	1 M KOH	1.61 V	10 mA cm^{-2}	45
CoFe@N–GCNCs–700	1 M KOH	1.63 V	10 mA cm^{-2}	46
$CoFe_2O_4$	1 M KOH	1.63 V	10 mA cm^{-2}	47
CoNiN@NiFe LDH	1 M KOH	1.63 V	10 mA cm^{-2}	48
CuFe Composite	1 M KOH	1.64 V	10 mA cm^{-2}	49
$NiCo_2O_4$	1 M KOH	1.65 V	10 mA cm^{-2}	14
FeCoS/C	1 M KOH	1.66 V	10 mA cm^{-2}	50
DLD–FeCoP@CNT	1 M KOH	1.67 V	10 mA cm^{-2}	51
Ni–Co–S/CF	1 M KOH	1.67 V	10 mA cm^{-2}	52
$NiMoP_2$	1 M KOH	1.67 V	10 mA cm^{-2}	53
FeCoP	1 M KOH	1.68 V	10 mA cm^{-2}	54
Ni/MoN@NCNT/CC	1 M KOH	1.69 V	10 mA cm^{-2}	55
NiS/MoS_2	1 M KOH	1.69 V	10 mA cm^{-2}	56
$NiCo_2O_4$	1 M KOH	1.72 V	10 mA cm^{-2}	57
Cu_2S–Ni_3S_2	1 M KOH	1.77 V	10 mA cm^{-2}	58

Co–Fe binary oxide	1 M KOH	1.92 V	10 mA cm^{-2}	59
Ni–Fe–Doped $K_{0.23}MnO_2$	1 M KOH	1.62 V	10 mA cm^{-2}	60
Fe–Ni–Cr	1 M KOH	1.64 V	10 mA cm^{-2}	61
Te/Fe–NiOOH	1 M KOH	1.65 V	10 mA cm^{-2}	62
Fe–Ni_2P/MoS_x/NF	1 M KOH	1.68	10 mA cm^{-2}	63
Fe_xNi_y/CeO_2	1 M KOH	1.70 V	10 mA cm^{-2}	64
CoFeNiO	1 M KOH	1.96 V	10 mA cm^{-2}	65

Table S6 Experimental volume (EV), theoretical volume (TV) and Faradaic efficiency (FE) of H_2 and O_2.

Time (min)	EV_{H2} (mL)	EV_{O2} (mL)	TV_{H2} (mL)	TV_{O2} (mL)	FE_{H2}(%)	FE_{O2}(%)
0	2.00	2.00	2.00	2.00	–	–
5	3.14	2.56	3.15	2.57	99.13	98.25
10	4.30	3.13	4.31	3.15	99.56	98.25
15	5.45	3.70	5.47	3.73	99.42	98.25
20	6.70	4.26	6.63	4.31	101.51	97.83
25	7.85	4.81	7.78	4.89	101.21	97.23
30	9.00	5.46	8.94	5.47	100.86	99.71

Note S1:

For HER in 1M KOH electrolyte:

$$H_2O + e^- \rightarrow *H + OH^- (Volmer\ reaction)$$

$$H_2O + e^- + *H \rightarrow H_2 + OH^- (Heyrovsky\ reaction)$$

$$*H + *H \rightarrow H_2 (Tafel\ reaction)$$

$$2H_2O + 2e^- \rightarrow H_2 + 2\,\mathrm{OH}^- (Total\ reaction)$$

For OER in 1M KOH electrolyte (Sabatier's adsorbate evolution mechanism):

$$H_2O + * \rightarrow *OH + H^+ + e^-$$

$$*OH \rightarrow *O + H^+ + e^-$$

$$*O + OH^- \rightarrow *OOH + e^-$$

$$*OOH \rightarrow * + O_2 + H^+ + e^-$$

* and X* represent an adsorption site and an adsorbed X intermediate on the surface, respectively.

Note S2:

TOF values are calculated according to previous method.[66]

$$TOF = \frac{N_{total}}{N_{active\ sites}}$$

where N_{total} is the number of total hydrogen turnovers per geometric area, and $N_{active\ sites}$ is the number of active sites per geometric area. The values of N_{total} and $N_{active\ sites}$ are calculated according to the equations:

$$N_{total} = j(\frac{mA}{cm^2})(\frac{1C_s^{-1}}{1000\,mA})(\frac{1mol\,H_2}{2\,mol\,e^-})(\frac{6.022\times10^{23}\,H_2\,molecules}{1mol\,H_2})$$

$$N_{active\ sites} = (\frac{No.of\ atoms/unit\,cell}{Volume/unit\,cell})^{\frac{2}{3}}$$

For the FeS, the volume of unit cell is 70.515 Å^3. the volume of unit cell containing 2 Fe atom and 2 S atom. The $N_{active\ sites}$ is determined to be 1.47×10^{15} atoms cm^{-2}.

$$ECSA = \frac{C_{dl}}{C_s}$$

where C_{dl} and C_s represent the double layer capacitance and specific capacitance, respectively. C_s=40 μF cm^{-2}.

$$A_{ECSA}^{FS2} = \frac{195.5\,mF\,cm^{-2}}{40\,\mu F\,cm^{-2}\ per\,cm^2_{ECSA}} = 4887.5\,cm^2_{ECSA}$$

$$A_{ECSA}^{FZS2} = \frac{284.9\,mF\,cm^{-2}}{40\,\mu F\,cm^{-2}\ per\,cm^2_{ECSA}} = 7122.5\,cm^2_{ECSA}$$

$$A_{ECSA}^{FMS2} = \frac{242.4\,mF\,cm^{-2}}{40\,\mu F\,cm^{-2}\ per\,cm^2_{ECSA}} = 6060\,cm^2_{ECSA}$$

$$A_{ECSA}^{FMZS2} = \frac{360.1\,mF\,cm^{-2}}{40\,\mu F\,cm^{-2}\ per\,cm^2_{ECSA}} = 9002.5\,cm^2_{ECSA}$$

At 200 mV overpotential, the current density of FS2 is 16.82 mA cm^{-2}.

$$TOF(\mathrm{FS2}) = \frac{3.12\times10^{15}\times16.82}{1.47\times10^{15}\times4887.5} = 7.30\times10^{-3}\,s^{-1}$$

At the overpotential of 200 mV, the current density of FMZS2 is 56.31 mA cm^{-2}.

$$TOF(\mathrm{FMZS2}) = \frac{3.12\times10^{15}\times56.31}{1.47\times10^{15}\times9002.5} = 0.013\,s^{-1}$$

Note S3:

Faradaic efficiency (FE) values are calculated as:[67-69]

$$V_{theoretical} = \frac{i \times t \times V_m}{n \times F}$$

$$FE(\%) = \frac{V_{experimental}}{V_{theoretical}}$$

where i is the current, t is the time, V_m is the molar volume of gas, n is the number of electrons in the reaction and F is the Faraday constant.

References

1. D.-Y. Wang, M. Gong, H.-L. Chou, C.-J. Pan, H.-A. Chen, Y. Wu, M.-C. Lin, M. Guan, J. Yang, C.-W. Chen, Y.-L. Wang, B.-J. Hwang, C.-C. Chen and H. Dai, *J. Am. Chem. Soc.*, 2015, **137**, 1587-1592.
2. H. Li, S. Chen, H. Lin, X. Xu, H. Yang, L. Song and X. Wang, *Small*, 2017, **13**, 1701487.
3. Z. Huang, Z. Chen, Z. Chen, C. Lv, M. G. Humphrey and C. Zhang, *Nano Energy*, 2014, **9**, 373-382.
4. S. Singh, D. C. Nguyen, N. H. Kim and J. H. Lee, *Chem. Eng. J.*, 2022, **442**.
5. Y. Liu, Y. Bai, Y. Han, Z. Yu, S. Zhang, G. Wang, J. Wei, Q. Wu and K. Sun, *ACS Appl. Mater. Interfaces*, 2017, **9**, 36917-36926.
6. T. Duy Thanh, H. Van Hien, L. Huu Tuan, N. H. Kim and J. H. Lee, *J. Mater. Chem. A*, 2020, **8**, 14746-14756.
7. X. Peng, L. Hu, L. Wang, X. Zhang, J. Fu, K. Huo, L. Y. S. Lee, K.-Y. Wong and P. K. Chu, *Nano Energy*, 2016, **26**, 603-609.
8. Y. Gu, A. Wu, Y. Jiao, H. Zheng, X. Wang, Y. Xie, L. Wang, C. Tian and H. Fu, *Angew Chem Int Edit*, 2021, **60**, 6673-6681.
9. C. Lv, X. Wang, L. Gao, A. Wang, S. Wang, R. Wang, X. Ning, Y. Li, D. W. Boukhvalov, Z. Huang and C. Zhang, *ACS Catal.*, 2020, **10**, 13323-13333.
10. F. Jing, Q. Lv, J. Xiao, Q. Wang and S. Wang, *J. Mater. Chem. A*, 2018, **6**, 14207-14214.
11. X. Liu, W. Liu, M. Ko, M. Park, M. G. Kim, P. Oh, S. Chae, S. Park, A. Casimir, G. Wu and J. Cho, *Adv. Funct. Mater.*, 2015, **25**, 5799-5808.
12. L. Jiang, N. Yang, C. Yang, X. Zhu, Y. Jiang, X. Shen, C. Li and Q. Sun, *Appl Catal B-environ*, 2020, **269**, 118780.
13. H. Su, S. Song, S. Li, Y. Gao, L. Ge, W. Song, T. Ma and J. Liu, *Appl Catal B-environ*, 2021, **293**, 120225.
14. X. Gao, H. Zhang, Q. Li, X. Yu, Z. Hong, X. Zhang, C. Liang and Z. Lin, *Angew Chem Int Edit*, 2016, **55**, 6290-6294.
15. W. Hao, R. Wu, R. Zhang, Y. Ha, Z. Chen, L. Wang, Y. Yang, X. Ma, D. Sun, F. Fang and Y. Guo, *Adv. Energy Mater.*, 2018, **8**, 1801372.
16. A. Muthurasu, V. Maruthapandian and H. Y. Kim, *Appl Catal B-environ*, 2019, **248**, 202-210.
17. J. Hu, C. Zhang, L. Jiang, H. Lin, Y. An, D. Zhou, M. K. H. Leung and S. Yang, *Joule*, 2017, **1**, 383-393.
18. Y. Hou, M. R. Lohe, J. Zhang, S. Liu, X. Zhuang and X. Feng, *Energy Environ. Sci.*, 2016, **9**, 478-483.
19. P. Babar, A. Lokhande, V. Karade, B. Pawar, M. G. Gang, S. Pawar and J. H. Kim, *J. Colloid Interface Sci.*, 2019, **537**, 43-49.
20. D. Zhao, H. Liu and X. Wu, *Nano Energy*, 2019, **57**, 363-370.
21. W.-l. Xiong, M. I. Abdullah and M.-m. Ma, *Chinese Journal of Chemical Physics*, 2018, **31**, 806-812.
22. K. S. Joya, M. A. Ehsan, N.-U.-A. Babar, M. Sohail and Z. H. Yamani, *J. Mater. Chem. A*, 2019, **7**, 9137-9144.
23. M. Yang, J.-Y. Xie, Z.-Y. Lin, B. Dong, Y. Chen, X. Ma, M.-L. Wen, Y.-N. Zhou, L. Wang and Y.-M. Chai, *Appl. Surf. Sci.*, 2020, **507**, 145096.

24. X. Huang, S. Wang, X. Zhang and L. Liu, *International Journal of Electrochemical Science*, 2021, **16**, 210433.
25. S. H. Park, S. H. Kang and D. H. Youn, *Materials*, 2021, **14**, 4768.
26. Y. Liu, Y. Liu, Y. Yu, C. Liu and S. Xing, *Frontiers in Energy*, 2022, **16**, 483-491.
27. Z. Guo, X. Wang, F. Yang and Z. Liu, *J. Alloy. Compd.*, 2022, **895**, 162614.
28. R. G. Jadhav, D. Singh, P. V. Krivoshapkin and A. K. Das, *Inorg. Chem.*, 2020, **59**, 7469-7478.
29. K. Patil, P. Babar, D. M. Lee, V. Karade, E. Jo, S. Korade and J. H. Kim, *Sustainable Energy Fuels*, 2020, **4**, 5254-5263.
30. T. E. Seuferling, T. R. Larson, J. M. Barforoush and K. C. Leonard, *ACS Sustainable Chem. Eng.*, 2021, **9**, 16678-16686.
31. M. Xing, L.-B. Kong, M.-C. Liu, L.-Y. Liu, L. Kang and Y.-C. Luo, *J. Mater. Chem. A*, 2014, **2**, 18435-18443.
32. Y. Hao, G. Du, Y. Fan, L. Jia, D. Han, W. Zhao, Q. Su, S. Ding and B. Xu, *ACS Appl. Mater. Interfaces*, 2021, **13**, 55263-55271.
33. G. Chen, D. Chen, J. Huang, C. Zhang, W. Chen, T. Li, B. Huang, T. Shao, J. Li and K. K. Ostrikov, *ACS Appl. Mater. Interfaces*, 2021, **13**, 45566-45577.
34. J.-F. Qin, M. Yang, S. Hou, B. Dong, T.-S. Chen, X. Ma, J.-Y. Xie, Y.-N. Zhou, J. Nan and Y.-M. Chai, *Appl. Surf. Sci.*, 2020, **502**, 144172.
35. R. Badrnezhad, F. Nasri, H. Pourfarzad and S. K. Jafari, *Int. J. Hydrogen Energy*, 2021, **46**, 3821-3832.
36. T. Li, T. Jing, D. Rao, X. Jia, Y. Zuo, S. Kment and R. Zboril, *J. Mater. Chem. A*, 2021, **9**, 12283-12290.
37. X. Wu, L. He and X. Wang, *Ceram. Int.*, 2021, **47**, 25755-25762.
38. R. Ding, S. Cui, J. Lin, Z. Sun, P. Du and C. Chen, *Catal. Sci. Technol.*, 2017, **7**, 3056-3064.
39. J. Shi, J. Hu, Y. Luo, X. Sun and A. M. Asiri, *Catal. Sci. Technol.*, 2015, **5**, 4954-4958.
40. A. Z. Alhakemy, A. B. A. A. Nassr, A. E.-H. Kashyout and Z. Wen, *Sustainable Energy Fuels*, 2022, **6**, 1382-1397.
41. B. Qiu, A. Han, D. Jiang, T. Wang and P. Du, *ACS Sustainable Chem. Eng.*, 2019, **7**, 2360-2369.
42. T. Linh, S.-K. Jerng, S. B. Roy, J. H. Jeon, K. Kim, K. Akbar, Y. Yi and S.-H. Chun, *ACS Sustainable Chem. Eng.*, 2019, **7**, 4625-4630.
43. W. Fang, D. Liu, Q. Lu, X. Sun and A. M. Asiri, *Electrochem. Commun.*, 2016, **63**, 60-64.
44. L. Zhang, L. Xie, M. Ma, F. Qu, G. Du, A. M. Asiri, L. Chen and X. Sun, *Catal. Sci. Technol.*, 2017, **7**, 2689-2694.
45. T. Bhowmik, M. K. Kundu and S. Barman, *ACS Appl. Energy Mater.*, 2018, **1**, 1200.
46. H.-J. Niu, Y.-P. Chen, R.-M. Sun, A.-J. Wang, L.-P. Mei, L. Zhang and J.-J. Feng, *J. Power Sources*, 2020, **480**, 229107.
47. B. Debnath, S. Parvin, H. Dixit and S. Bhattacharyya, *Chemsuschem*, 2020, **13**, 3875-3886.
48. J. Wang, G. Lv and C. Wang, *Appl. Surf. Sci.*, 2021, **570**, 151182.
49. A. I. Inamdar, H. S. Chavan, B. Hou, C. H. Lee, S. U. Lee, S. Cha, H. Kim and H. Im, *Small*, 2020, **16**, 1905884.
50. W. Wang, Y. Xu, J. Yao, X. Liu, Z. Yin and Z. Li, *Dalton Transactions*, 2020, **49**, 13352-13358.

51. B. Wang, Y. Chen, Q. Wu, Y. Lu, X. Zhang, X. Wang, B. Yu, D. Yang and W. Zhang, *J Mater Sci Technol*, 2021, **74**, 11-20.
52. T. Liu, X. Sun, A. M. Asiri and Y. He, *Int. J. Hydrogen Energy*, 2016, **41**, 7264-7269.
53. X.-D. Wang, H.-Y. Chen, Y.-F. Xu, J.-F. Liao, B.-X. Chen, H.-S. Rao, D.-B. Kuang and C.-Y. Su, *J. Mater. Chem. A*, 2017, **5**, 7191-7199.
54. K. L. Sun, K. H. Wang, T. P. Yu, X. Liu, G. X. Wang, L. H. Jiang, Y. Y. Bu and G. W. Xie, *Int. J. Hydrogen Energy*, 2019, **44**, 1328-1335.
55. P. Wang, J. Qi, C. Li, X. Chen, T. Wang and C. Liang, *Chemelectrochem*, 2020, **7**, 00023.
56. Y. Zheng, P. Tang, X. Xu and X. Sang, *J. Solid State Chem.*, 2020, **292**, 121644.
57. R. Zhao, D. Cui, J. Dai, J. Xiang and F. Wu, *Sustainable Materials and Technologies*, 2020, **24**, e00151.
58. K. S. Bhat and H. S. Nagaraja, *Chemistryselect*, 2020, **5**, 2455-2464.
59. W. Adamson, X. Bo, Y. Li, B. H. R. Suryanto, X. Chen and C. Zhao, *Catal. Today*, 2020, **351**, 44-49.
60. H. Liao, X. Guo, Y. Hou, H. Liang, Z. Zhou and H. Yang, *Small*, 2020, **16**, 1905223.
61. J. Zhang, H. Jang, L. L. Chen, X. L. Jiang, M. G. Kim, Z. X. Wu, X. Liu and J. Cho, *Mater. Chem. Phys.*, 2020, **241**, 122375.
62. S. Ibraheem, X. T. Li, S. S. A. Shah, T. Najam, G. Yasin, R. Iqbal, S. Hussain, W. Y. Ding and F. Shahzad, *ACS Appl. Mater. Interfaces*, 2021, **13**, 10972-10978.
63. X. L. Zhang, C. Liang, X. Y. Qu, Y. F. Ren, J. J. Yin, W. J. Wang, M. S. Yang, W. Huang and X. C. Dong, *Advanced Materials Interfaces*, 2020, **7**, 1901926.
64. L. Chen, H. Jang, M. G. Kim, Q. Qin, X. Liu and J. Cho, *Inorganic Chemistry Frontiers*, 2020, **7**, 470-476.
65. Y. He, D. Aasen, A. McDougall, H. Yu, M. Labbe, C. Ni, S. Milliken, D. G. Ivey and J. G. C. Veinot, *Chemelectrochem*, 2021, **8**, 1391-1392.
66. Z. Chen, Y. Song, J. Cai, X. Zheng, D. Han, Y. Wu, Y. Zang, S. Niu, Y. Liu, J. Zhu, X. Liu and G. Wang, *Angewandte Chemie-International Edition*, 2018, **57**, 5076-5080.
67. S. Yang, J.-Y. Zhu, X.-N. Chen, M.-J. Huang, S.-H. Cai, J.-Y. Han and J.-S. Li, *Appl. Catal. B-Environ.*, 2022, **304**, 120914.
68. G. Zhou, X. Wu, M. Zhao, H. Pang, L. Xu, J. Yang and Y. Tang, *Chemsuschem*, 2021, **14**, 699-708.
69. J. Zhang, H. Zhou, Y. Liu, J. Zhang, Y. Cui, J. Li, J. Lian, G. Wang and Q. Jiang, *ACS Appl. Mater. Interfaces*, 2021, **13**, 52598-52609.